

# Structurally distinct endocytic pathways for B cell receptors in B lymphocytes

Aleah D. Roberts<sup>†</sup>, Thaddeus M. Davenport<sup>†</sup>, Andrea M. Dickey, Regina Ahn, Kem A. Sochacki, and Justin W. Taraska\*

Biochemistry and Biophysics Center, National Heart, Lung, and Blood Institute, National Institutes of Health, Bethesda, MD 20892

**ABSTRACT** B lymphocytes play a critical role in adaptive immunity. On antigen binding, B cell receptors (BCR) cluster on the plasma membrane and are internalized by endocytosis. In this process, B cells capture diverse antigens in various contexts and concentrations. However, it is unclear whether the mechanism of BCR endocytosis changes in response to these factors. Here, we studied the mechanism of soluble antigen-induced BCR clustering and internalization in a cultured human B cell line using correlative superresolution fluorescence and platinum replica electron microscopy. First, by visualizing nanoscale BCR clusters, we provide direct evidence that BCR cluster size increases with F(ab')<sub>2</sub> concentration. Next, we show that the physical mechanism of internalization switches in response to BCR cluster size. At low concentrations of antigen, B cells internalize small BCR clusters by classical clathrin-mediated endocytosis. At high antigen concentrations, when cluster size increases beyond the size of a single clathrin-coated pit, B cells retrieve receptor clusters using large invaginations of the plasma membrane capped with clathrin. At these sites, we observed early and sustained recruitment of actin and an actin polymerizing protein FCHSD2. We further show that actin recruitment is required for the efficient generation of these novel endocytic carriers and for their capture into the cytosol. We propose that in B cells, the mechanism of endocytosis switches to accommodate large receptor clusters formed when cells encounter high concentrations of soluble antigen. This mechanism is regulated by the organization and dynamics of the cortical actin cytoskeleton.

## Monitoring Editor

Mary Munson  
University of Massachusetts  
Medical School

Received: Aug 14, 2020

Revised: Sep 29, 2020

Accepted: Oct 5, 2020

## INTRODUCTION

B lymphocytes are critical in adaptive immune responses to pathogens (Trombetta and Mellman, 2005). Dysregulation of B cell activity can lead to cancer, autoimmunity, and allergy (Avalos et al., 2014). The B cell receptor (BCR), abundant in the plasma membrane of B cells, binds to and internalizes antigens by endocytosis for processing and presentation to T cells (Clark et al., 2004; Harwood and

Batista, 2010). BCR activation, along with T cell engagement, promotes the expansion of a clonal lineage of antigen-specific B cells. As a first step, clustering of BCRs in response to antigen binding initiates a signaling cascade that triggers the internalization of receptor/antigen complexes by endocytosis (Harwood and Batista, 2010; Pierce and Liu, 2010). Antigen structure, concentration, and

This article was published online ahead of print in MBoC in Press (<http://www.molbiolcell.org/cgi/doi/10.1091/mbc.E20-08-0532>) on October 21, 2020.

Author contributions: A.D.R., T.M.D. and J.W.T. designed experiments; T.M.D. performed molecular biology, confocal, FACS, and TIRF experiments for initial characterization of the system; A.D.R. performed molecular biology, confocal internalization assays, TIRF, SIM, and STORM experiments characterizing the role of actin in BCR stimulation; T.M.D., A.M.D., and K.A.S. performed platinum replica TEM and CLEM experiments; K.A.S. designed and wrote analysis software; R.A. and A.D.R. did thin section TEM; A.D.R., T.M.D., and J.W.T. wrote the manuscript, and all authors commented on work; J.W.T. oversaw the project.

<sup>†</sup>Co-first authors.

\*Address correspondence to: Justin W. Taraska ([justin.taraska@nih.gov](mailto:justin.taraska@nih.gov)).

Abbreviations used: BCR, B cell receptor; BSA, bovine serum albumin; CCS, clathrin-coated structure; CIE, clathrin-independent endocytosis; CLEM,

correlative light electron microscopy; dSTORM, direct stochastic optical reconstruction microscopy; Dyn, Dynamin; EGF, epidermal growth factor; EGFR, epidermal growth factor receptor; FACS, fluorescence assisted cell sorting; FCHSD2, FCH and double SH3 domain containing protein 2; CME, clathrin-mediated endocytosis; MFI, mean fluorescence intensity; PBS, phosphate-buffered saline; PFA, paraformaldehyde; SIM, structured illumination microscopy; SRM, smooth raised membrane; TEM, transmission electron microscopy.

© 2020 Roberts et al. This article is distributed by The American Society for Cell Biology under license from the author(s). Two months after publication it is available to the public under an Attribution-NonCommercial-Share Alike 3.0 Unported Creative Commons License (<http://creativecommons.org/licenses/by-nc-sa/3.0>).

"ASCB®," "The American Society for Cell Biology®," and "Molecular Biology of the Cell®" are registered trademarks of The American Society for Cell Biology.

presentation may all influence the size of BCR/antigen clusters formed on the plasma membrane (Batista *et al.*, 2001; Thyagarajan *et al.*, 2003; Srinivas Reddy *et al.*, 2011). The radii of these clusters can vary from ~60 nm to over 1  $\mu\text{m}$  (Pierce and Liu, 2010; Lee *et al.*, 2017; Stone *et al.*, 2017). The membrane trafficking pathways that enable B cells to specifically internalize antigen in spite of such structural variability are unclear.

Clathrin-mediated endocytosis (CME) is the primary mechanism of endocytosis in eukaryotic cells (Conner and Schmid, 2003; McMahon and Boucrot, 2011; Mettlen *et al.*, 2018). In CME, a complex of adaptors, accessory proteins, lipids, and cargo recruit clathrin to the inner leaflet of the plasma membrane where it assembles as a lattice that curves and drives the formation of vesicles (McMahon and Boucrot, 2011; Mettlen *et al.*, 2018). Clathrin has been shown to play an important role in BCR endocytosis and BCR signaling (Salisbury *et al.*, 1980; Stoddart *et al.*, 2005; Natkanski *et al.*, 2013). For example, knockdown of clathrin dramatically impairs BCR internalization (Stoddart *et al.*, 2005). Similarly, mutations of clathrin-adaptor domains found in the BCR complex results in active receptors that accumulate at the plasma membrane and are observed in lymphomas (Davis *et al.*, 2010). The precise role of clathrin in BCR endocytosis, however, is not well defined.

While clathrin has been shown to be important for BCR endocytosis, B cells can retrieve BCRs in the absence of clathrin (Stoddart *et al.*, 2005). This raises the possibility that there may be other mechanisms of BCR internalization. A number of alternative endocytic pathways have been described in eukaryotic cells (Mayor *et al.*, 2014; Watanabe and Boucrot, 2017). These clathrin-independent endocytosis (CIE) pathways include micron-scale pinocytosis and phagocytosis processes as well as nanometer-scale mechanisms such as caveolae, flotillin-based, endophilin-based, actin-based, and other less well-defined vesicle or transport processes (Mayor *et al.*, 2014; Ferreira and Boucrot, 2018). Thus, it is not known if CIE uptake pathways exist for BCRs or if a unique hybrid form of endocytosis operates during antigen-mediated BCR internalization. In support of other pathways, previous work has shown that B cells are capable of internalizing large cargos through a process akin to phagocytosis (Souwer *et al.*, 2009). This capacity for phagocytic-like processes is consistent with observations that actin and myosin play an important role in antigen-mediated BCR clustering, activation, and internalization (Brown and Song, 2001; Tolar, 2017). Furthermore, large pieces of B cell and target membranes are internalized when B cells interact with antigen presented on supported membranes (Natkanski *et al.*, 2013). Interestingly, this membrane capture process depends on clathrin, but doesn't appear to wholly resemble classic CME in size, structure, or molecular composition (Natkanski *et al.*, 2013).

How antigen concentration and receptor cluster size impact the proposed pathways of BCR endocytosis is also unclear. Concentration-dependent internalization mechanisms have been proposed for some receptors such as epidermal growth factor receptor (EGFR) (Tomas *et al.*, 2014). Low concentrations of epidermal growth factor (EGF) stimulate EGFR uptake by a clathrin-dependent mechanism, but at high EGF concentrations internalization occurs by a mixture of clathrin-dependent and clathrin-independent mechanisms (Sigismund *et al.*, 2008). Such behaviors have not been described for the BCR. However, B cells might benefit from such a concentration-dependent switch in the mechanism of BCR endocytosis. Specifically, by adjusting the endocytic mechanism of BCR uptake in response to antigen concentrations, B cells might be better able to rapidly and appropriately respond to a wide range of changes in the concentration of foreign antigens during an infection. Likewise, B

cells could avoid inappropriate or unnecessary responses to common self-antigens (e.g., leading to autoimmunity) or transient exposures to foreign but nonpathogenic molecules (e.g., leading to allergy). However, no systematic study has been made to directly visualize the nanoscale structural changes in the plasma membrane of B cells during antigen challenge.

Here, we study the formation and structure of anti-human IgM F(ab')<sub>2</sub>-induced endocytic carriers in the IgM+ DG-75 human B cell line to understand the mechanism of BCR internalization. Specifically, we investigated the role of clathrin in mediating BCR endocytosis across a range of antigen concentrations. First, we measure BCR internalization in live cells and observe the nanoscale structure and dynamics of antigen-induced BCR clustering and internalization in real time. Next, we use correlative superresolution fluorescence and platinum replica transmission electron microscopy (CLEM) to directly map the nanoscale architecture of BCR endocytic structures throughout the process of antigen stimulation and uptake. We show that BCR clusters induced by increasing concentrations of antigen and time are captured by distinct nanoscale plasma membrane invaginations capped with clathrin. We then show that these distinct plasma membrane structures recruit actin and that actin polymerization is important for the capture and internalization of large BCR clusters. This work provides direct evidence for the structural complexity of BCR endocytosis and offers direct insights into a novel endocytic mechanism that allows B cells to tailor their endocytic machinery to accommodate the wide range of BCR cluster sizes formed at the plasma membrane of living B cells.

## RESULTS

### Antigen stimulation across a wide range of concentrations induces efficient BCR internalization

First, to characterize the temporal and spatial dynamics of BCR internalization in our system, we imaged live DG-75 cells with confocal microscopy (Figure 1, a and b). Cross-linking anti-human IgM F(ab')<sub>2</sub> antibody was added to DG-75 cells to a final concentration of 12  $\mu\text{g}/\text{ml}$  at 37°C to induce activation and internalization of native BCRs pre-labeled at a low concentration with fluorescent single chain F(ab) fragments. Five minutes after the addition of the cross-linking ligand, cell-surface BCRs formed small fluorescent patches that condensed into larger clusters that were internalized into the cytoplasm over a period of 25 min (Figure 1, a and b). These results are consistent with previous studies of BCR clustering (Brown and Song, 2001). Furthermore, population-based fluorescence assisted cell sorting (FACS) measurements of receptor internalization indicated that BCRs were internalized across a wide range of stimulating antigen concentration (0.88–14  $\mu\text{g}/\text{ml}$  F(ab')<sub>2</sub>; Supplemental Figure S1 a–c). Here, similar amounts of fluorescently labeled BCR-bound F(ab) fragments were internalized at both low (2  $\mu\text{g}/\text{ml}$  F(ab')<sub>2</sub>) and high (8  $\mu\text{g}/\text{ml}$  F(ab')<sub>2</sub>) concentrations of stimulating antigen (Supplemental Figure S1d). These results were supported by thin section transmission electron microscopy (TEM) of B cells stimulated in the presence of membrane-bound ferritin, a small electron-dense indicator that labels the outer leaflet of the plasma membrane and the inner leaflet of endocytic vesicles. In unstimulated cells, little internalization of surface-bound ferritin was observed by thin section TEM (Supplemental Figure S2, a–c), but ferritin-positive endocytic structures were observed attached to the plasma membrane and deeper in the cytosol after cells were stimulated for 15 min with 8  $\mu\text{g}/\text{ml}$  anti-human IgM F(ab')<sub>2</sub> (Supplemental Figure S2, d and e).

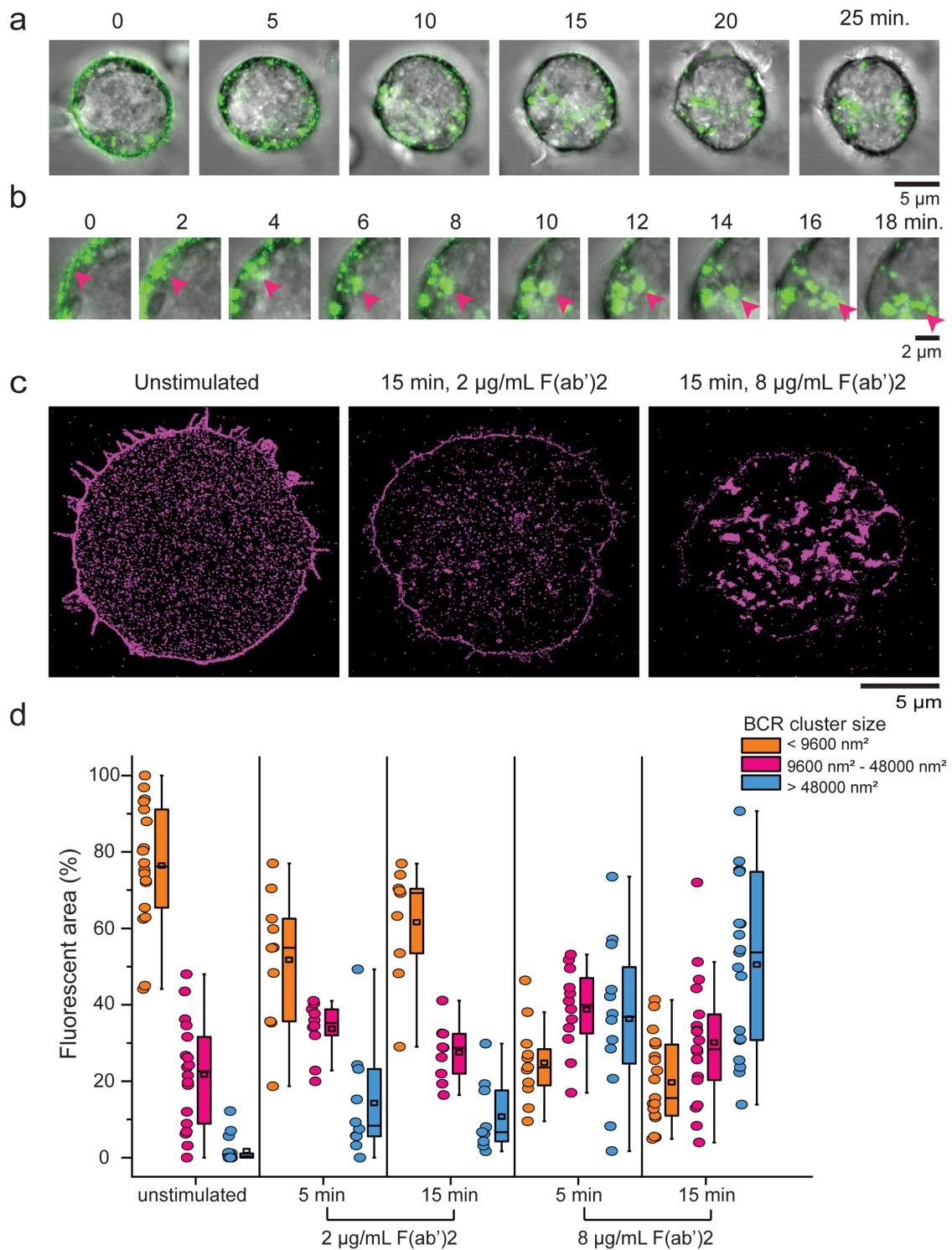


**FIGURE 1:** F(ab')<sub>2</sub> stimulation of DG-75 cells induces BCR clustering and internalization. (a) Confocal images of a live DG-75 cell labeled with anti-human IgM F(ab)-Alexa Fluor 488 and stimulated with 12 µg/ml anti-human IgM F(ab')<sub>2</sub> at t = 0 min. BCR is shown in green and transmitted light is grayscale. (b) Top left region of cell in a; pink arrow tracks BCRs that cluster and internalize into the cytoplasm. (c) Reconstructed superresolution images of the BCR (magenta) clustering on the bottom surface of DG-75 cells labeled with anti-human IgM F(ab)-Alexa Fluor 647 and left unstimulated or stimulated with anti-human IgM F(ab')<sub>2</sub> at either 2 or 8 µg/ml F(ab')<sub>2</sub> for 15 min prior to plating, fixation, and imaging. (d) Percentage of total fluorescent area in each cell composed of small (<9600 nm<sup>2</sup>, orange bar), intermediate (9600–48,000 nm<sup>2</sup>, pink bar), and large (>48,000 nm<sup>2</sup>, blue bar) punctae for unstimulated DG-75 cells; cells stimulated with 2 µg/ml F(ab')<sub>2</sub> for 5 or 15 min; and cells stimulated with 8 µg/ml F(ab')<sub>2</sub> for 5 or 15 min (n = unstimulated 18 cells—47,847 spots; 5 min 2 µg/ml 10 cells—23,728 spots; 5 min 8 µg/ml 12 cells—10,497 spots; 15 min 2 µg/ml 9 cells—14,347 spots; 15 min 8 µg/ml 19 cells—8237 spots). Plots show the mean (square), median (line), 25/75 percentile range (box), and outliers with a coefficient value of 1.5 and data points (circles) from each cell.

## BCR cluster size is dependent on concentration of F(ab')<sub>2</sub> stimulation

As a first step in BCR uptake, antigen-bound BCRs aggregate on the plasma membrane (Lee *et al.*, 2017). To determine whether the concentration of soluble ligand alters the nanoscale distribution and clustering of BCRs in the plasma membrane, we measured the size of BCR clusters using direct stochastic optical reconstruction microscopy (dSTORM), a superresolution localization microscopy method (Betzig *et al.*, 2006; Heilemann *et al.*, 2008). Figure 1c shows representative dSTORM images of DG-75 cells stained with Alexa 647-labeled anti-human IgM F(ab) fragments under three conditions: unstimulated, incubated with low (2  $\mu\text{g/ml}$ ), or high (8  $\mu\text{g/ml}$ ) concentrations of F(ab')<sub>2</sub> for 15 min at 37°C before attachment to coverslips and fixation. In unstimulated cells, BCR fluorescence was uniformly distributed across the plasma membrane with few measurable clusters (Figure 1c, left). After 15 min of stimulation with 2  $\mu\text{g/ml}$  F(ab')<sub>2</sub>, the size of BCR fluorescent spots increased (Figure 1c, center). However, the most dramatic change in BCR distribution was observed after 15 min of stimulation with 8  $\mu\text{g/ml}$  F(ab')<sub>2</sub>, which resulted in very large clusters of BCR fluorescence (Figure 1c, right).

As shown in Figure 1, after BCRs cluster they are endocytosed into the cytosol. To investigate the mechanism of endocytosis, we first classified these BCR clusters into three groups based on their size relative to one candidate endocytic carrier, clathrin-coated pits. Clathrin-coated pits have an area of around 18,000 nm<sup>2</sup> on average, but range from 10,000 to 50,000 nm<sup>2</sup> in area, or 55 to 125 nm in radius (Sochacki *et al.*, 2012, 2017; Dambournet *et al.*, 2018). Thus, using these sizes as a reference, we characterized: 1) small spots (<9600 nm<sup>2</sup>), which are smaller than a typical clathrin-coated pit; 2) intermediate spots (9600–48,000 nm<sup>2</sup>), which are comparable in size to the majority of clathrin-coated pits; and 3) large fluorescent spots (>48,000 nm<sup>2</sup>), which are over 2.5 times the mean area of clathrin-coated pits. Approximately 76% of the fluorescent area in unstimulated cells was composed of small spots, with a majority of the remaining made up of spots between 9600 and 48,000 nm<sup>2</sup> (Figure 1d). Large clusters made up an insignificant portion (around 2%) of the fluorescence in unstimulated cells. In contrast, for cells treated with 8  $\mu\text{g/ml}$  F(ab')<sub>2</sub>, large fluorescent spots made up an increasing large proportion of the fluorescent area (36 and 51%) at both the 5- and 15-min time points, respectively (Figure 1d). This was not the case for cells treated with 2  $\mu\text{g/ml}$  F(ab')<sub>2</sub>, in which 62% of the fluorescent area was made up of small spots, although there was a slightly increased proportion of intermediate and large fluorescent clusters relative to unstimulated cells (Figure 1d). Thus, increasing the concentration of soluble F(ab')<sub>2</sub> dramatically increased the size of BCR clusters on the plasma membrane. Of note, after 15 min of stimulation with 8  $\mu\text{g/ml}$  F(ab')<sub>2</sub>, we predominantly observed very large BCR clusters that exceeded the size of a typical clathrin-coated pit. If BCR clusters exceed the size of their proposed endocytic clathrin carriers, we next asked how these large clusters are captured and internalized.

## Large BCR clusters are associated with distinct endocytic structures at the plasma membrane

CLEM provides a unique nanoscale view of the cellular environment of proteins localized by fluorescence microscopy (Sochacki *et al.*, 2014; Kopek *et al.*, 2017). Figure 2, a and b show correlated super-resolution fluorescence and platinum replica EM image (CLEM image) of the inner plasma membrane of an unstimulated DG-75 B cell plasma membrane. Similar to the data shown in Figure 1c, BCR fluorescence in unstimulated cells was characterized by localizations distributed randomly across the plasma membrane. In platinum rep-

lica EM, the structure of plasma membrane-associated actin and vesicles are visible. No obvious association of the receptor with cytoskeletal filaments or vesicles was seen. Of note, cells generally exhibited a macroscopic ring pattern of membrane-associated actin. The CLEM images in Figure 2, c–f show the inner membrane of DG-75 cells after 5 min of stimulation with 2 or 8  $\mu\text{g/ml}$  F(ab')<sub>2</sub>.

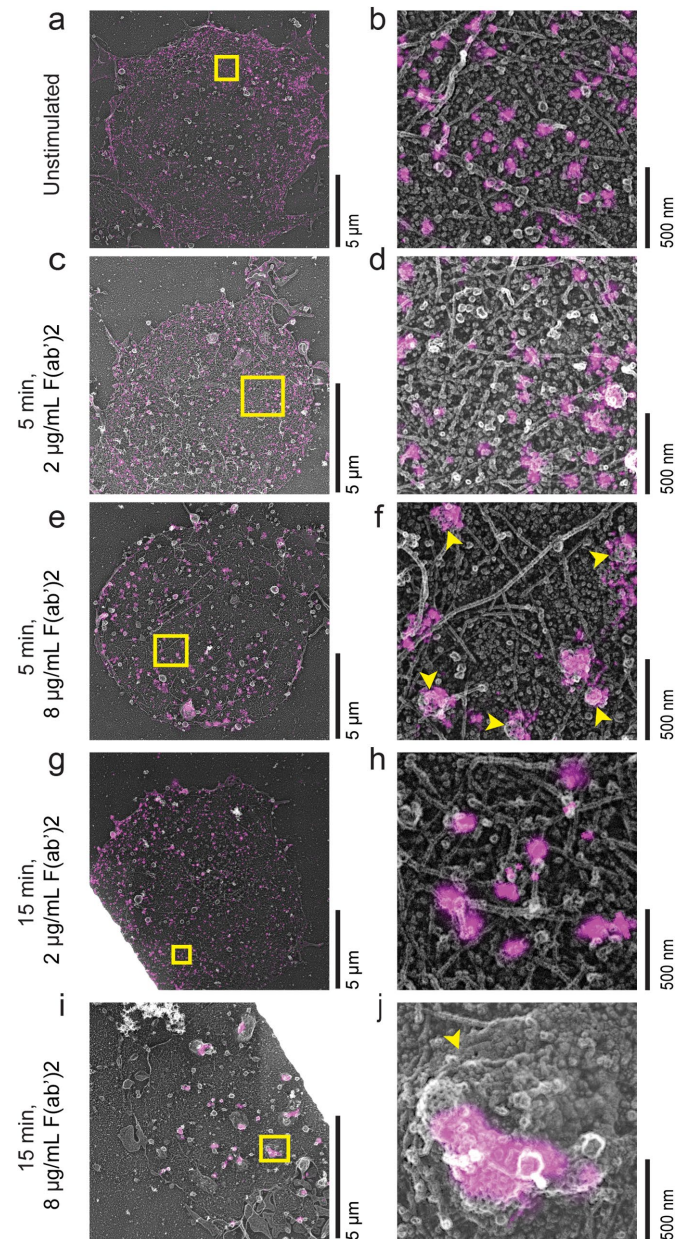


**FIGURE 2:** CLEM analysis of membrane changes during BCR clustering in DG-75 cells after stimulation. CLEM overlay images of DG-75 cells that have been unroofed and fixed before dSTORM and TEM imaging. For dSTORM imaging, cells were labeled with anti-human IgM F(ab)-Alexa Fluor 647. After d-STORM imaging, cells were prepared by PREM and imaged using a TEM microscope. Images in parts a, c, e, g, and i show the whole cell, and corresponding zoomed-in images of the regions in yellow boxes are shown in parts b, d, f, h, and j. The yellow arrows in part f point out regions of the plasma membrane that have BCR fluorescence associated with clathrin lattices. The yellow arrow in part j points out a smooth raised portion of the plasma membrane that has clathrin lattices and BCR fluorescence on it.

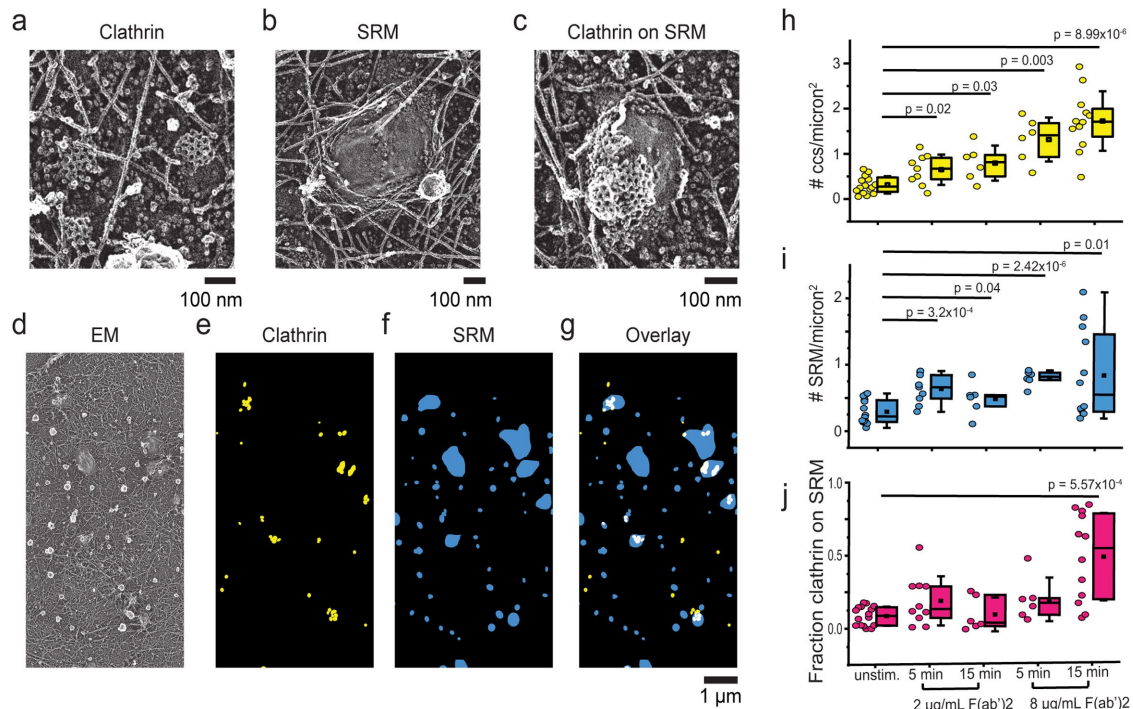


**FIGURE 3:** Changes in clathrin and SRM structures in TEM images following F(ab')<sub>2</sub> stimulation. Representative PREM images of clathrin (a), SRM structures (b), and clathrin on SRMs (c). (d) Example PREM image used for identification and resulting segmentation shown for (e) clathrin marked in yellow, (f) SRM structures as blue objects, and (g) an overlay with the clathrin found on SRM structures as white regions. These segmented masks were used to measure the change in the density of CCS (h) and SRM (i) on the membrane. Association of CCS and SRM structures was quantified in j. Box and whisker plots (h–j) show the mean (square), median (line), 25/75 percentile range (box), and outliers with a coefficient value of 1.5.

Unlike cells treated with 2 μg/ml F(ab')<sub>2</sub> (Figure 2, c and d), after 5 min of stimulation with 8 μg/ml F(ab')<sub>2</sub>, BCR clusters began to form, and these clusters were often associated with honeycomb clathrin lattices in the correlated TEM image (Figure 2, e and f; yellow arrows point to clathrin lattices with BCR fluorescence). After 15 min of stimulation with 8 μg/ml F(ab')<sub>2</sub>, BCR clusters were larger and were frequently correlated with dense honeycomb arrays that were often associated with distinctive smooth, raised regions of the plasma membrane (Figure 2, i and j; yellow arrow points to distinctive smooth raised structure with clathrin and BCR fluorescence). In contrast, cells treated with 2 μg/ml F(ab')<sub>2</sub> showed much smaller BCR fluorescence punctate and few morphological changes of the plasma membrane after 15 min (Figure 2, g and h).

To quantitatively track the changes in the membrane and organelles following antigen stimulation in B cells, we first analyzed the structure of regions of the plasma membrane in platinum replica TEM images (Figure 3). For this analysis we focused on identifying distinctive plasma membrane structures in stimulated cells. TEM images were segmented for two major objects: 1) honey-comb clathrin lattices (“Clathrin”) (Figure 3a) and 2) smooth, raised sections of the plasma membrane (smooth raised membrane [SRM]; Figure 3b). These two structures often colocalized as SRMs coated with clathrin (clathrin on SRMs; Figure 3c). Figure 3, d–f shows an example platinum replica TEM image (Figure 3d) and its corresponding segmented masks identifying clathrin (Figure 3e), SRM (Figure 3f), and clathrin on SRM structures (Figure 3g). Segmented masks were generated for each cell and used to quantitatively analyze the density of each structure on the plasma membrane (Figure 3, h–j). This analysis shows that the density of clathrin-coated structures (CCS) is very low in unstimulated DG-75 cells (0.31 CCS/μm<sup>2</sup> ± 0.05 SEM)

relative to other mammalian cell types (Figure 3h). For example, PC12 cells have ~1.6 CCS/μm<sup>2</sup> (Sochacki *et al.*, 2012). Treatment with 8 μg/ml F(ab')<sub>2</sub> dramatically increased the amount of clathrin on the plasma membrane: at the 5-min time point, we measured 1.32 CCS/μm<sup>2</sup> ± 0.2 SEM and 1.73 CCS/μm<sup>2</sup> ± 0.19 SEM after 15 min. There was less recruitment of clathrin to the plasma membrane following treatment with 2 μg/ml F(ab')<sub>2</sub>: at 5 min, we measured a density of 0.65 CCS/μm<sup>2</sup> ± 0.11 SEM that only mildly increased at 15 min (0.79 CCS/μm<sup>2</sup> ± 0.16 SEM; Figure 3 h). Of note, individual clathrin structures did not change in size, with the average Feret size of clathrin structures remaining constant across stimulations (Supplemental Figure S3a). But individual spots did group together, showing a closer nearest-neighbor distance than would be expected from the increased density of clathrin observed over the course of activation (Supplemental Figure S3b). Figure 3i shows that the density of SRMs also increased during stimulation with the largest increase in SRMs seen after 15 min in cells exposed to 8 μg/ml F(ab')<sub>2</sub>. Like clathrin, these structures did not change in overall diameter (Supplemental Figure S3c) and yet, different from clathrin, showed only moderate clustering (Supplemental Figure S3d). Figure 3j shows that in many cases, CCS directly associated with SRMs. The most dramatic overlap of clathrin and SRMs was observed in cells treated for 15 min with 8 μg/ml F(ab')<sub>2</sub>. Thus, high concentrations of F(ab')<sub>2</sub> induce the formation of large smooth invaginations of the plasma membrane that contain clusters of small CCS.

### BCR clusters are located on distinct clathrin on SRM structures

The above analysis was performed on platinum replica TEM images to understand the impact of antigen activation on the morphology

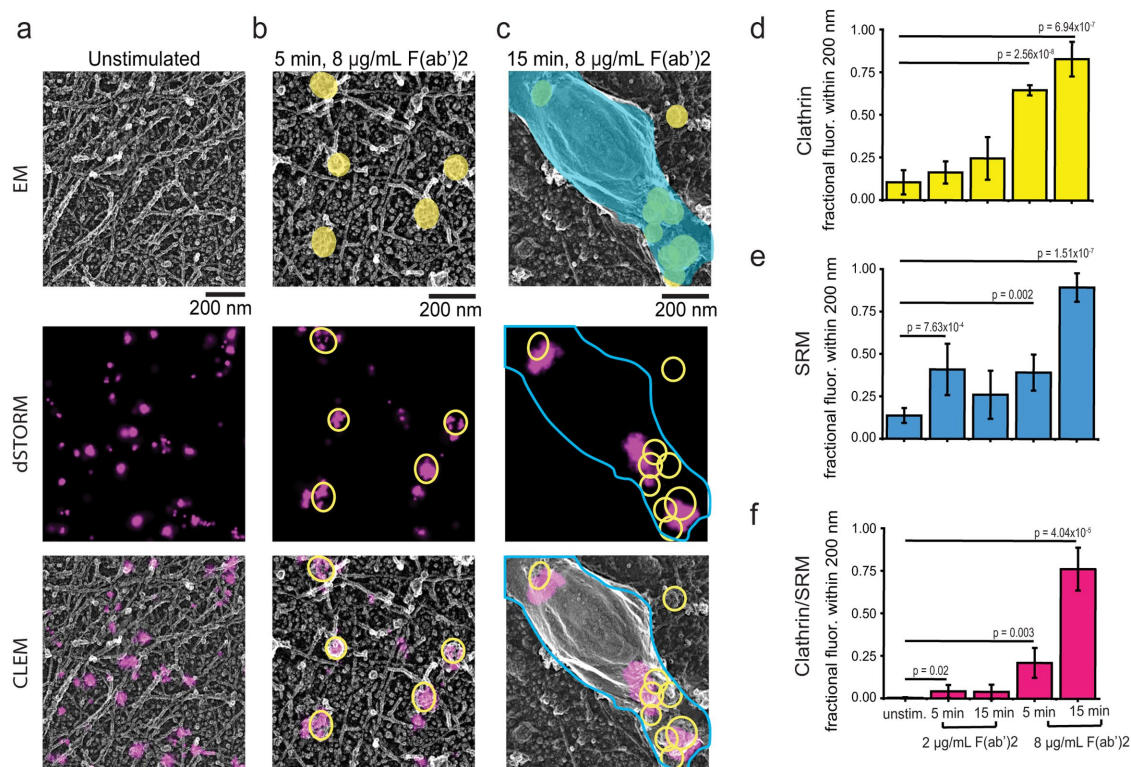


**FIGURE 4:** Analysis of changes in the distribution of BCR fluorescence relative to CCS and SRM structures in CLEM images following F(ab')<sub>2</sub> stimulation. Example CLEM images (gray, EM; magenta, dSTORM; and overlay) of (a) unstimulated, (b) 5 min sample, and (c) 15 min sample of cells stimulated with 8 µg/ml F(ab')<sub>2</sub>. Plots of the fraction of BCR fluorescence measured in an 1800 nm total radius located within 200 nm of a (d) CCS, (e) SRM, or (f) Clathrin on SRM for five different experimental conditions measured from CLEM images. After 5 min of stimulation with 8 µg/ml F(ab')<sub>2</sub>, approximately 70% of all BCR fluorescence is found within 200 nm of CCS, and after 15 min of stimulation with 8 µg/ml F(ab')<sub>2</sub> nearly 80% of all BCR fluorescence is found within 200 nm of clathrin on SRM structures. Bar graph shows mean ± SD (n = Unstim. 5 cells, 5 min 2 µg/ml 9 cells, 5 min 8 µg/ml 6 cells, 15 min 2 µg/ml 6 cells, and 15 min 8 µg/ml 6 cells).

and structure of the plasma membrane. Next, we quantified changes in the distribution of BCR fluorescence on the plasma membrane relative to these EM-identified locations using superresolution CLEM images. As seen in the CLEM images (Figure 4, a–c), BCR fluorescence did not always exclusively overlap with clathrin but was often found both on clathrin and in the areas closely surrounding clathrin (additional images of clathrin on SRM structures and BCR fluorescent overlays are shown in Supplemental Figure S4). Thus, using the segmented objects shown in Figure 4 to identify both the directly bound and closely associated fluorescence, we measured the fraction of BCR fluorescence within a 200-nm radius of three different segmented plasma membrane regions (clathrin, SRM, and clathrin located on SRMs) in five different experimental conditions (unstimulated, 5 min 2 µg/ml F(ab')<sub>2</sub>, 5 min 8 µg/ml F(ab')<sub>2</sub>, 15 min 2 µg/ml F(ab')<sub>2</sub>, and 15 min 8 µg/ml F(ab')<sub>2</sub>). The 200-nm radius was chosen to include all of the structure-associated fluorescence and was based on empirical analysis of mean fluorescence versus distance (Supplemental Figure S5). Figure 4, d–f shows that in unstimulated cells, few BCR fluorescent localizations were associated with clathrin, SRMs, or clathrin on SRMs. However, stimulation with 8 µg/ml F(ab')<sub>2</sub> for 5 min resulted in a concentration of BCR fluorescence within 200 nm of both clathrin and SRM structures, which further increased at 15 min. As shown in Figure 3, under these conditions, most clathrin is found grouped on SRMs, and thus, our measurements in Figure 4f likewise show that the majority of BCR fluorescence is concentrated on and around these SRM-localized clathrin clusters. In contrast, cells treated

with 2 µg/ml F(ab')<sub>2</sub> showed less association of BCR fluorescence with SRM-associated clathrin (Figure 4f). It should be noted that there was little clathrin observed on SRMs under these conditions. Another point of interest in these data is that when cells are stimulated at 8 µg/ml F(ab')<sub>2</sub>, clathrin is more highly localized near BCR clusters at the 5-min time point than SRM structures. SRM structures are not similarly associated with BCR clusters until between 5 and 15 min after stimulation. This suggests that clathrin is recruited to BCR clusters before SRM structures are generated.

#### Actin is recruited early to BCR clusters stimulated with a high concentration of F(ab')<sub>2</sub>

To identify proteins that may be important for generation of the novel clathrin on SRM structures, we used TIRF microscopy to study the colocalization of a panel of candidate endocytic proteins (clathrin, actin, endophilins A1 and A2, synaptojanin 2, and FCHSD2) with BCRs when cells were stimulated with 2 or 8 µg/ml F(ab')<sub>2</sub> (Supplemental Figure S6). Based on our previous data, at the lower concentration of stimulating antigen, BCRs are localized in single CCS, and at the high concentrations of antigen, BCR clusters are predominantly localized in and around clustered clathrin on SRM structures. Other proteins were imaged but here we are focusing on proteins that exhibited differences in localization between the two concentrations. Our data show that both actin and Endophilin A1 were significantly recruited to BCR clusters stimulated with 8 µg/ml F(ab')<sub>2</sub> at the 15-min time point. Endophilin A1 is thought to be expressed

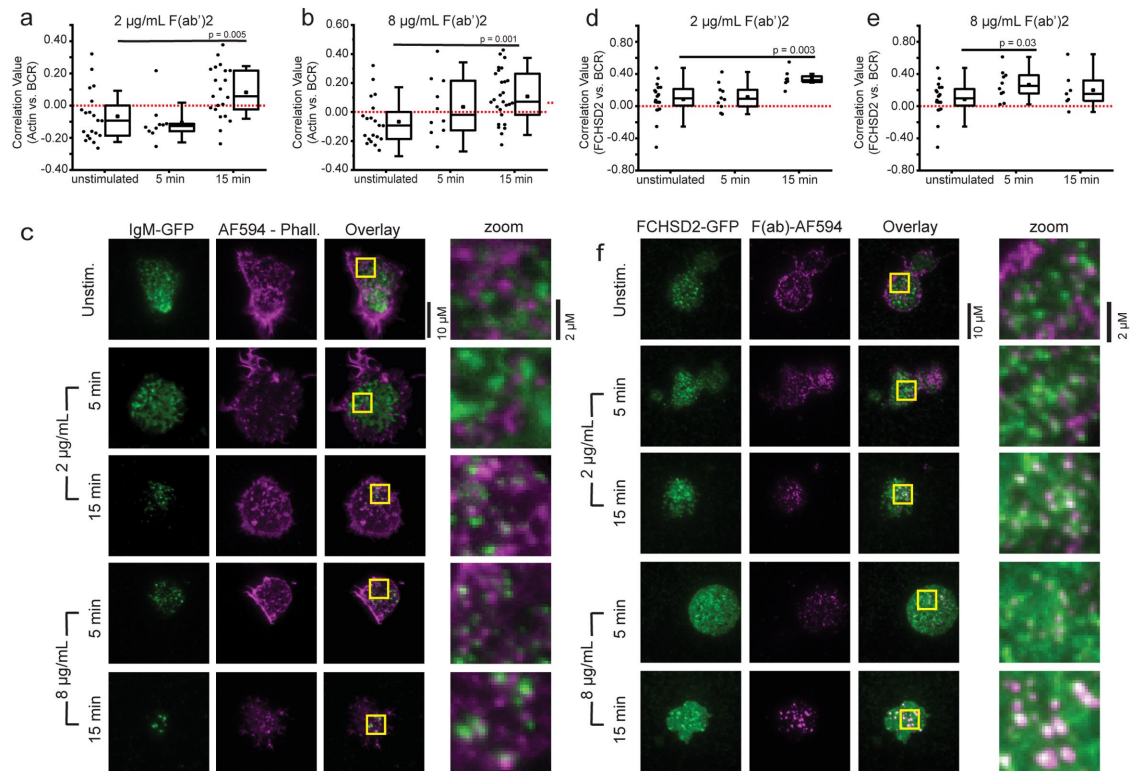


**FIGURE 5:** Actin is recruited early to BCR clusters stimulated with a high concentration of F(ab)'2. (a) Colocalization analysis of the BCR (IgM-GFP overexpression) and actin (stained with Alexa Fluor 594-phalloidin) in DG-75 cells stimulated with 2  $\mu\text{g}/\text{mL}$  F(ab)'2 for 5 or 15 min. (b) The same colocalization analysis done in a is shown for cells treated with 8  $\mu\text{g}/\text{mL}$  F(ab)'2 for 5 or 15 min. (c) Representative TIRF microscopy images from the colocalization analysis presented in a and b. The zoomed images are from the regions highlighted in yellow boxes. (d) Colocalization analysis of the BCR (labeled with Alexa Fluor 594-F(ab) fragment) and FCHSD2 (FCHSD2-GFP overexpression) in DG-75 cells stimulated with 2  $\mu\text{g}/\text{mL}$  F(ab)'2 for 5 or 15 min. (e) The same colocalization analysis done in d is shown for cells treated with 8  $\mu\text{g}/\text{mL}$  F(ab)'2. (f) Representative TIRF microscopy images from the colocalization analysis presented in d and e. All of the box plots from a, b, d, and e show the mean (square), median (line), 25/75 percentile range (box), and outliers with a coefficient value of 1.5 and data points (circles) from each cell.

predominantly in neurons (Ringstad *et al.*, 1997). We, however, could not detect endogenous expression of Endophilin A1 in DG-75 cells with Western blotting. For this reason, we did not further study a role of Endophilin A1. The cortical actin cytoskeleton, however, has been reported to play an important role in BCR clustering and activation in B cells. Specifically, with stimulation, actin has been shown to remodel to allow increased mobilization and clustering of BCRs (Hao and August, 2005; Treanor *et al.*, 2010, 2011; Freeman *et al.*, 2011). BCR clustering facilitated by actin reorganization is essential for efficient signalosome formation and subsequent cell activation (Harwood and Batista, 2010; Liu *et al.*, 2012; Ketchum *et al.*, 2014). Actin is also involved in the movement of BCR-containing vesicles from the early to late endosome after internalization (Brown and Song, 2001). In light of the enhanced recruitment of actin we observed in Supplemental Figure S6 and previous work suggesting a role for actin in BCR clustering and activation, we decided to further investigate the role of actin in BCR endocytosis at these novel clathrin on SRM structures. We likewise pursued the role of FCH and double SH3 domain containing protein 2 (FCHSD2). This protein has been shown to be involved in generating f-actin at sites of classical clathrin-mediated endocytosis, is found in B cells, and has been associated as a risk factor in autoimmune diseases (Lessard *et al.*, 2016; Almeida-Souza *et al.*, 2018; Rodal *et al.*, 2008).

We analyzed actin colocalization with the BCR over 15 min in DG-75 cells stimulated with either 2 or 8  $\mu\text{g}/\text{mL}$  F(ab)'2 (Figure 5, a–c).

Cells stimulated with 2  $\mu\text{g}/\text{mL}$  F(ab)'2 did not show significant colocalization of the BCR with actin until the late 15-min time point. However, stimulation with 8  $\mu\text{g}/\text{mL}$  F(ab)'2 induced colocalization of BCRs and actin as early as 5 min, and this colocalization continued to increase until the 15-min time point. Thus, with strong antigen stimulation, actin appears to be recruited to large BCR clusters early. This suggests a role for actin in endocytosis of large BCR clusters that is different from its role in classical clathrin-mediated endocytosis. Figure 5c shows representative images of cells expressing the BCR fused to GFP and stained with phalloidin to mark filamentous actin. Of note, we observed that in unstimulated cells, or cells stimulated with 2  $\mu\text{g}/\text{mL}$  F(ab)'2, actin filaments are mostly arranged around the footprint of the cell (Figure 5c, top three rows). After stimulation with 8  $\mu\text{g}/\text{mL}$  F(ab)'2 for 15 min, however, actin appears to reorganize and move away from the footprint and assemble around BCR clusters at the plasma membrane (Figure 5c, bottom row).

Next, we analyzed the localization of FCHSD2 in relation to clathrin and BCRs. Consistent with previous reports, FCHSD2 is highly colocalized with clathrin (Supplemental Figure S7). We also observed colocalization of FCHSD2 with BCR clusters generated by 2 or 8  $\mu\text{g}/\text{mL}$  F(ab)'2 (Figure 5, d–f). Figure 5f shows representative images of cells expressing FCHSD2 fused to GFP and stained with anti-IgM F(ab) to mark the localization of the BCR. At the 5-min time point, FCHSD2 is more highly correlated with BCR clusters

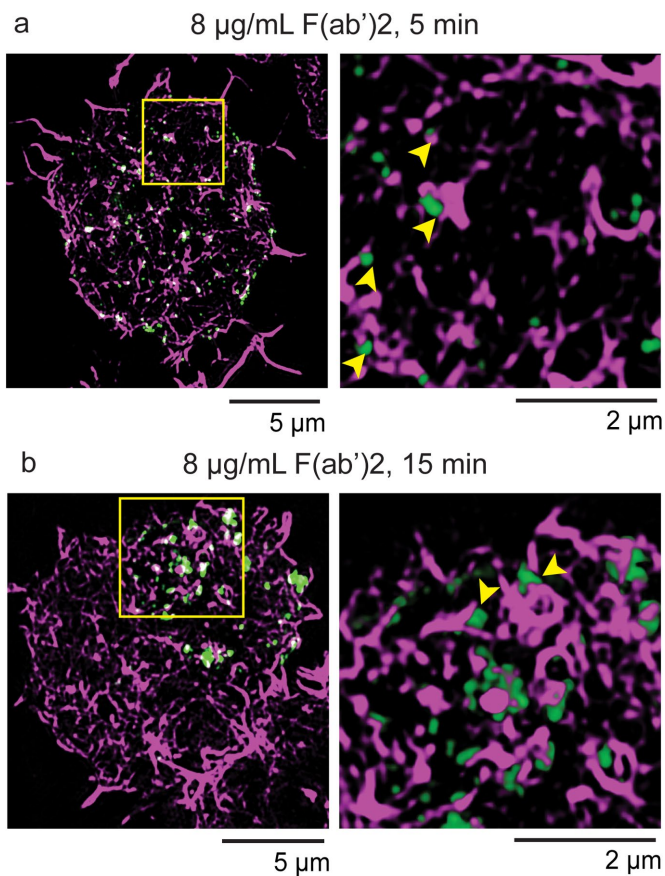


**FIGURE 6:** Superresolution images of actin interaction with BCR clusters. (a, b) 3D SIM of cells treated with 8 µg/ml F(ab')<sub>2</sub> for 5 or 15 min. DG-75 cells were transfected to express IgM-GFP and then stained with Alexa Fluor 594-phalloidin after stimulation. Zoomed images correspond to regions in yellow boxes. Yellow arrows in a show early points of contact between actin and the BCR clusters. The yellow arrows in b show basket like actin structures formed around BCR clusters.

stimulated with 8 µg/ml rather than 2 µg/ml. These data are consistent with actin and the actin polymerization machinery being specifically recruited to large BCR clusters.

The above data show that actin and FCHSD2 have distinct recruitment kinetics in cells stimulated with 8 µg/ml F(ab')<sub>2</sub>. Both proteins are recruited to BCR clusters stimulated with 8 µg/ml F(ab')<sub>2</sub> at an early time point. This is not due to a differential recruitment of clathrin, because clathrin is recruited to BCR clusters with similar kinetics at 2 or 8 µg/ml F(ab')<sub>2</sub> (Supplemental Figure S8). This differential recruitment suggests that both actin and FCHSD2 may have distinct functional roles in endocytosis of large BCR clusters. Based on these data, we hypothesize that clathrin and FCHSD2 act together on SRM structures to activate actin polymerization and endocytosis at the early 5-min time point. At the 15-min time point, when cells are treated with 8 µg/ml F(ab')<sub>2</sub> actin continues to colocalize with the BCR while FCHSD2 colocalization begins to decline. This suggests that FCHSD2 may only be involved in recruiting actin for the early stages of SRM formation and not for internalization at the later stage. While we show that FCHSD2 clearly colocalizes with clathrin, future perturbation studies on the role of FCHSD2 in BCR endocytosis are needed to prove a direct mechanistic role for FCHSD2 in polymerizing actin at SRMs.

Next, to gain a more detailed view of the interaction between actin and the BCR cluster in stimulated cells, we used 3D structured illumination microscopy (SIM) to obtain a subdiffraction level view of how actin interacts with BCR clusters (Figure 6, a and b). After 5 min of treatment with 8 µg/ml F(ab')<sub>2</sub>, we observed actin filaments making close contact with many developing BCR clusters (Figure 6a, yellow arrows). At the 15-min time point (Figure 6b), we observed actin filaments reorganize around larger BCR clusters to form basket like structures (yellow arrows) that surround the receptors.

Together these data show that significant changes in the organization of actin occur after stimulation with a high concentration of F(ab')<sub>2</sub>. Specifically, BCR clusters colocalize with the f-actin activating protein FCHSD2 and actin (Figure 5) and forms basketlike structures around BCR clusters (Figure 6). We hypothesize that structural changes in the localization and arrangement of actin are essential for the formation of smooth raised structure on the membrane capped with clathrin. Next, we tested this hypothesis by perturbing the formation of filamentous actin using the actin-disrupting drug Cytochalasin D.

### Actin filaments are essential for efficient formation of clathrin on SRM structures and internalization of large BCR clusters

To perturb the cortical cytoskeleton we used the f-actin-destabilizing drug Cytochalasin D to determine what stage of large BCR cluster internalization requires actin: 1) receptor clustering, or 2) formation of clathrin on SRM structures or 3) internalization. We analyzed the effects on receptor clustering using direct STORM localization microscopy to study the BCR. We measured the cluster sizes of unstimulated DG-75 cells or cells stimulated with 8 µg/ml F(ab')<sub>2</sub> in the presence or absence of Cytochalasin D (Figure 7a). As expected, in unstimulated cells there were few large BCR clusters. On average only about 1% of total fluorescence in unstimulated cells was in large clusters. In contrast, cells treated with 8 µg/ml F(ab')<sub>2</sub> alone or stimulated in the presence of Cytochalasin D generated large BCR clusters at similar increased relative percentages (44% and 45% respectively; Figure 7b). These results are consistent with previous reports that actin depolymerization is needed to increase BCR mobilization at the plasma membrane and promote receptor clustering (Hao and August, 2005; Treanor *et al.*, 2010, 2011; Freeman *et al.*, 2011). Likewise, these data indicate that filamentous actin is not necessary to drive BCR clustering.

We next used PREM to analyze the effect of Cytochalasin D on the structure and density of clathrin and SRMs at the plasma membrane (Figure 7, c–e). TEM images of membranes from cells that were left untreated, stimulated with 8 µg/ml F(ab')<sub>2</sub> alone, or stimulated in the presence of Cytochalasin D were segmented to identify clathrin and SRM structures (representative images of clathrin and SRM segmentation are presented in Supplemental Figure S9, a–d). In stimulated cells, the density of both clathrin and SRM structures increased compared with untreated cells, and this effect was blocked by Cytochalasin D treatment (Figure 7, c and d). Consistent with these results, the fraction of SRM structures with clathrin associated also decreased when cells were treated with Cytochalasin D, indicating a partial inhibitory effect of Cytochalasin D on clathrin/SRM structure biogenesis (Figure 7e). Interestingly, some clathrin on SRM structures were still present in cells treated with Cytochalasin D. This suggests that additional proteins other than actin are involved in the generation of clathrin/SRM structures or that the block of actin's actions with Cytochalasin D was partial. We also observed less clustering and a larger average radius of both clathrin and SRM structures in cells treated with Cytochalasin D (Supplemental Figure S9, e–h).

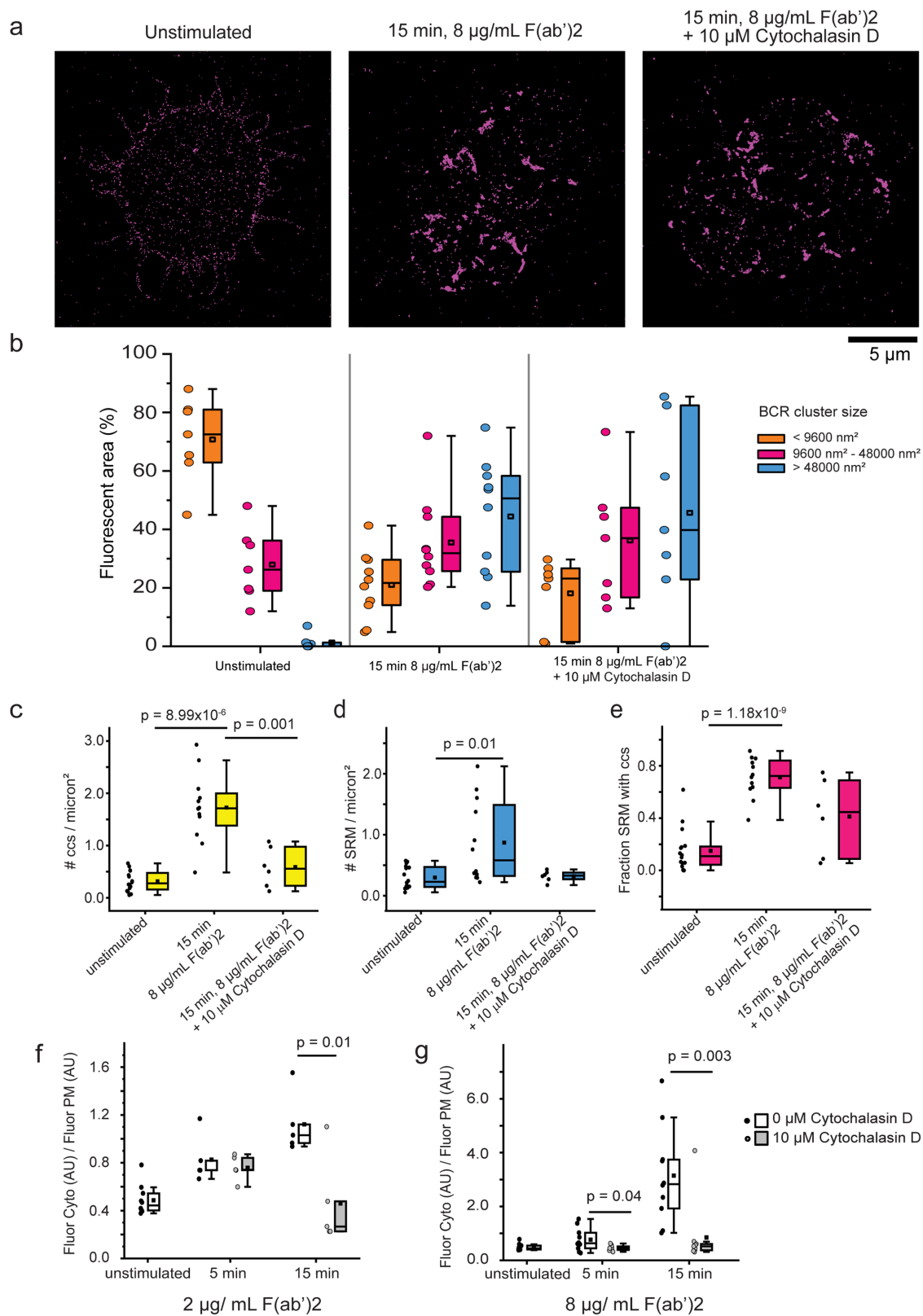


**FIGURE 7:** Cytochalasin D blocks efficient biogenesis and internalization of clathrin on SRM structures.

(a) Representative reconstructed dSTORM images of BCR clustering on the bottom surface of DG-75 cells labeled with anti-human IgM F(ab)-Alexa Fluor 647 (magenta) and left unstimulated, stimulated with 8  $\mu\text{g}/\text{mL}$  F(ab')<sub>2</sub> alone or stimulated with 8  $\mu\text{g}/\text{mL}$  F(ab')<sub>2</sub> in the presence of Cytochalasin D for 15 min prior to plating, fixation, and imaging.

(b) Percentage of the total fluorescent area composed of small (<9600 nm<sup>2</sup>, orange bar), intermediate (9600–48,000 nm<sup>2</sup>, pink bar), and large (>48,000 nm<sup>2</sup>, blue bar) puncta for cells stimulated under the conditions shown in part a ( $n$  = unstimulated 7 cells—15,050 spots, 15 min 8  $\mu\text{g}/\text{mL}$  10 cells—5676 spots, 15 min 8  $\mu\text{g}/\text{mL}$  + Cytochalasin D 7 cells—3914

Finally, we tested the effect of cytochalasin D on internalization of BCRs with a fluorescent internalization assay (Figure 7, f and g). At low concentration of F(ab')<sub>2</sub> stimulation, BCR internalization was inhibited after 15 min of stimulation (Figure 7f). In contrast, cells stimulated with a high concentration of F(ab')<sub>2</sub> were sensitive to Cytochalasin D treatment at the earlier 5-min time point (Figure 7g). The robust and rapid inhibition of BCR internalization into the cytosol of cells stimulated with high concentrations of ligand suggests that actin is essential for late steps in endocytosis. Together, our data indicate that actin has a complex mechanistic role in the formation and internalization of these specialized endocytic structures in B cells. Specifically, actin is preferentially recruited at an early time point in cells stimulated with high concentrations of ligand and is required for the efficient biogenesis of clathrin on SRM structures. Furthermore, the almost complete block of internalization indicates that either fission or transport of large BCR clusters into the cytosol is actin dependent.

## DISCUSSION

Adaptive immunity depends on the ability of B cells to capture antigen through a regulated internalization mechanism of the BCR (Harwood and Batista, 2010; Hoogeboom and Tolar, 2016). Here, we provide direct structural evidence that the mechanism of BCR captures changes with the concentration of the stimulating ligand and the resulting changes in size of BCR clusters. In unstimulated cells, BCR is evenly distributed across the plasma membrane. The plasma membrane in these cells contains few CCS compared with other mammalian cell types. On antigen stimulation at low concentration, BCRs cluster and associate with an increased number of classical CCS which are likely able to internalize these small BCR clusters using the standard clathrin-mediated endocytosis pathway. At higher antigen concentrations and longer times, however, large clathrin-associated BCR clusters coalesce onto SRM invaginations of the plasma membrane. FCHSD2 and actin colocalize with these large BCR clusters within minutes and forms cuplike structures around the clusters. Organized actin is required for internalization of these large BCR clusters into the cytosol. Our data support a model where B cells can accommodate the internalization of a wide range of BCR cluster sizes by deploying either classic clathrin-mediated endocytosis or a hybrid form of endocytosis that uses clathrin coats to gather receptors onto large membrane carriers to capture receptors wholesale into the cytoplasm. The latter is distinctly sensitive to actin disruption at an early time point. We also observed large differences in the recruitment of endocytic machinery in cells stimulated with low or high concentrations of F(ab')<sub>2</sub> (Figure 3) while not observing large changes in the total amount of internalization (Supplemental Figure S1d). We predict that when small BCR clusters form they are primarily taken up by clathrin endocytic machinery that is maintained at the plasma membrane without a large recruitment of new clathrin or SRM structures. Under high levels of stimulation, however, when large BCR clusters are generated on the plasma membrane, we hypothesize that there is a switch in the endocytic

mechanism that is needed to allow the cells to capture large clusters of the BCR. This alternate mechanism requires recruitment of more clathrin and the formation of SRM structures but does not necessarily lead to a greater number of receptors being internalized. We hypothesize that this plasticity of endocytic mechanisms allows cells to accomplish the uptake of these very large receptor clusters during strong stimulation regimes.

The role of actin in the formation and internalization of large BCR clusters is complex. Our data suggest that actin plays two mechanistic roles. First, at the early time points actin is recruited to BCR clusters, possibly by the FCHSD2 protein. FCHSD2 has been shown in other studies to activate actin polymerization (Almeida-Souza *et al.*, 2018; Rodal *et al.*, 2008). At this stage actin plays a role in supporting increased clathrin recruitment to the plasma membrane and in the formation of SRM structures (Figure 7, c and d). At later stages, actin is essential for internalization of SRM structures into the cytosol (Figure 7g). Although this dual role of actin in endocytosis of large BCR clusters was unexpected, it is not unprecedented for endocytic proteins to play more than one role in capturing surface receptors. For example, the GTPase Dynamin has been extensively studied for its role in driving membrane scission at late stages of clathrin-mediated endocytosis (Mettlen *et al.*, 2018). Specifically, two isoforms of Dynamin (Dyn1 and Dyn2) play unique roles at the early and late stages of clathrin-mediated endocytosis (Srinivasan *et al.*, 2018). Dyn1 controls the early initiation of clathrin-coated pits while Dyn2 drives membrane scission at the late stage of clathrin-mediated endocytosis.

We consider several implications of our finding on the B cell endocytic machinery. First, in unstimulated cells, most BCR was not associated with clathrin. Nor were there many clathrin structures present at the membrane. Most mammalian cells maintain a dynamic population of CCS at the membrane at a density between 0.5 and 2 structures per square micron (Taylor *et al.*, 2011; Sochacki *et al.*, 2012; Dambournet *et al.*, 2018). These structures support constitutive endocytosis and the recycling of many key receptors such as the transferrin receptor. We find that resting B cells maintain very few clathrin structures at their plasma membrane. This could serve to increase the steady-state concentration of BCRs on the surface. In contrast to unstimulated cells, most BCR fluorescence was associated with clathrin structures in cells treated with 8 µg/ml F(ab')<sub>2</sub> for 15 min. The relative absence of BCR-negative clathrin-coated pits suggests that clathrin assembles specifically on antigen-induced BCR clusters. Disruption of the actin cytoskeleton, however, inhibits clathrin recruitment to the plasma membrane. These data imply that BCR stimulation alone is not sufficient to induce clathrin recruitment, but this process also requires f-actin assembly at the plasma membrane. Considering the need for immune responses to be specific, regulated, and rapid, the lack of membrane-associated clathrin structures in resting B cells could serve as a barrier to limit BCR endocytosis and minimize off-target or autoimmune responses that might occur as a result of nonspecific antigen internalization (Davis *et al.*, 2010). Furthermore, the selective recruitment of clathrin to

---

spots). For c–e, cells were stimulated as indicated and then unroofed, and processed by PREM before TEM imaging. TEM images were segmented as previously described for Figure 3, and the density of clathrin (c) and SRM structures (d) is shown. (e) The fraction of SRM structures that have clathrin on them (representative masks used for generating these data are shown in Supplemental Figure S9). (f, g) Cells were stimulated with (f) 2 µg/ml or (g) 8 µg/ml F(ab')<sub>2</sub> alone (closed black circles and open box) or in the presence of 10 µM Cytochalasin D (gray circles and box) before fixation and imaging with a confocal microscope. BCR internalization is presented as the relative fluorescence in the cytoplasm divided by the fluorescence identified at the plasma membrane in a central z-slice for each cell. All Box and whisker plots in this figure show the mean (square), median (line), 25/75 percentile range (box), and outliers with a coefficient value of 1.5.

clustered BCR would ensure specific and efficient internalization of the target antigen.

Second, clathrin-associated BCR clusters form and group together in a concentration-dependent manner following F(ab')<sub>2</sub> stimulation. Treatment with 2 µg/ml F(ab')<sub>2</sub> stimulates efficient BCR internalization by flow cytometry, and this internalization appears to involve clathrin based on colocalization of BCR with clathrin in confocal microscopy images (Supplemental Figure S1e). However, CLEM data showed that this does not yield dramatic growth of BCR clusters or recruit large amounts of additional clathrin to the plasma membrane. In contrast, after 5 min of stimulation with 8 µg/ml F(ab')<sub>2</sub>, the amount of clathrin at the surface membrane increases and nearly all BCR clusters are associated with clathrin. After 15 min of stimulation with 8 µg/ml F(ab')<sub>2</sub>, BCR clusters capped with clathrin increase in number, cluster together, and are found to be largely associated with smooth, raised membrane structures. Thus, individual clathrin structures precede the development of SRMs capped with clathrin and BCRs. These data suggest a model in which relatively small BCR clusters may be internalized through a classic clathrin-mediated endocytic pathway, and BCR clusters that grow too large to be contained in a small clathrin-coated vesicle could require a hybrid mechanism of membrane internalization that involves bulk plasma membrane remodeling and early recruitment of actin. Given the large body of literature that supports a role for lipid microdomains in BCR signaling, one avenue for future work is to examine whether the smooth, raised structures we observe by CLEM form as a result of phase transitions within the plasma membrane (Cheng *et al.*, 1999; Sezgin *et al.*, 2017; Stone *et al.*, 2017).

From this model, we suggest that BCR clusters of different sizes would pose distinct challenges for the endocytic machinery and may therefore recruit distinct sets of regulatory proteins in each case. Whereas small BCR clusters may be internalized by a basic set of clathrin-associated proteins, perhaps larger BCR clusters depend on an expanded set of endocytic proteins (Watanabe and Boucrot, 2017; Ferreira and Boucrot, 2018). In support of this theory, we have shown that large BCR clusters rely on increased involvement of actin for internalization. This is analogous to what very large antigens appear to do in a mechanism that more closely resembles phagocytosis (Zhu *et al.*, 2016). Our survey of endocytic proteins in Supplemental Figure S6 also identified some proteins that are differentially recruited to small and large BCR clusters and could be further investigated. Additionally, previous work has shown that B cells rely on myosin to a greater extent when internalizing antigen presented on a bilayer compared with soluble antigen (Natkanski *et al.*, 2013). Similar to these studies, which show context and antigen-dependent variability in the mechanism of BCR uptake, our data support the hypothesis that BCR cluster composition and size may be another key factor that impacts the mechanism of BCR internalization in B cells.

We have shown that endocytic structures associated with large BCR clusters exhibit a unique nanoscale morphology at the plasma membrane. These structures exhibit dense, closely packed arrays of small clathrin structures on smooth, raised membrane invaginations. These clathrin-coated sites are unlike those observed by EM in other mammalian cell types (Sochacki *et al.*, 2014, 2017; Dambournet *et al.*, 2018; Scott *et al.*, 2018). However, there is some similarity between the raised clathrin structures we observe in B cells and the structures that form on mast cells in response to FCεRI clustering (Aggeler and Werb, 1982; Wilson *et al.*, 2002; Cleyrat *et al.*, 2013). There is overlap in the BCR and FCεRI signaling cascades (Siraganian *et al.*, 2010), and the morphological similarity we observe in the receptors' endocytic structures suggests that there may be com-

monalities in their mechanisms of internalization as well. Future work will be needed to determine the identity of other molecules that drive and regulate the proteins required for biogenesis of smooth, raised structures at the plasma membrane.

Our data support the idea that BCR endocytosis occurs by an adaptable mechanism, employing different nanoscale endocytic structures to internalize BCR clusters of different sizes. It remains to be determined whether these distinct endocytic structures traffic differently throughout the cell and what proteins might be employed to specifically drive these invaginations. Future studies to understand whether these structurally distinct endocytic pathways influence the efficiency of antigen processing and presentation will be valuable to ensure that future adjuvants and immunogens are optimally designed to cooperate with the available B cell endocytic machinery.

## MATERIALS AND METHODS

### Cell lines and imaging reagents

The IgM+VκL+ human DG-75 B cell line was purchased from ATCC (CRL-2625) and cultured in a growth medium consisting of RPMI 1640 (-) Phenol red with 10% fetal bovine serum, 1% penicillin/streptomycin, 10 mM HEPES, pH 7.4, and 1 mM sodium pyruvate. Cells were periodically tested for mycoplasma. Cell line identity was verified as a human B cell (ATCC). Anti-human IgM F(ab) and F(ab')<sub>2</sub> fragments were purchased from Jackson ImmunoResearch Laboratories, including: Goat anti-human IgM Fc5µ F(ab)-Fluorescein (109-097-043), Goat anti-human IgM Fc5µ F(ab)-Alexa Fluor 647 (109-607-043), Goat anti-human IgM Fc5µ F(ab)-Alexa Fluor 488 (109-547-043), Goat anti-human IgM Fc5µ F(ab)-Alexa Fluor 594 (109-587-043), and AffiniPure F(ab')<sub>2</sub> Fragment Goat anti-human IgG + IgM (H+L) (109-006-127). Fixable Viability Dye eFluor450 (65-0863-18), Alexa Fluor 488 phalloidin (A12379), mouse anti-clathrin heavy chain antibody clone X-22 (MA1065), and donkey anti-mouse Alexa Fluor647 (A31571) were purchased from ThermoFisher. Coverslips for TIRF and confocal microscopy #1.5 25 mm were purchased from Warner Instruments (64-0715), and high density (400 particles /100 mm<sup>2</sup>) wide spectral band (600 ± 100 nm) gold fiducial coverslips were purchased from Hestzig LLC. for correlative fluorescence electron microscopy. Coverslips were washed in a heated solution of hydrogen peroxide and ammonia solution as previously described (Trexler and Taraska, 2017) with gold fiducial coverslips exposed to the cleaning solution for 10 min. Poly-L-lysine for coating coverslips was purchased from Sigma Aldrich (P4832).

### Construction of DG-75 IgM-GFP

The DG-75 IgM V<sub>H</sub> sequence (GenBank: Z74668; Chapman *et al.*, 1996) with the native VH3-23\*01 leader peptide sequence (IMGT: M99660; Matsuda *et al.*, 1993) was synthesized by Biobasic and cloned by overlap PCR in frame with the human IGHM sequence obtained from DNASU (HscD00445046). This fragment was then cloned by overlap PCR upstream of a PCR product encoding meGFP with an SGS GSGSGSGSGGGPVAT N-terminal linker peptide. PCR reactions were carried out using Accuprime Pfx Supermix (ThermoFisher: 12344040) with primers synthesized by Integrated DNA Technologies. The DG75-V<sub>H</sub>-IgM-linker-GFP insert was digested with *NheI*/*NotI* and ligated into the Clontech pEGFP-N1 vector.

### Flow cytometry-based BCR internalization assay

DG-75 cells at a concentration of 1–1.5 million cells /ml were spun down at 200 × *g* for 5 min. The cell pellet was resuspended at 10 million cells/ml in a staining medium of RPMI complete with the addition of 1:1000 anti-human IgM F(ab)-FITC, 1:1000 anti-human

IgM-F(ab)-Alexa Fluor 647, and 1:1000 eFluor450 LIVE/DEAD Violet. Cells were stained at 4°C for 30 min prior to washing with RPMI complete and pelleting cells at 200 × g for 5 min. The stained, washed cell pellet was resuspended to a concentration of 2 million cells/ml in RPMI complete, filtered through a 40-µm filter, and 700 µl of cells were aliquoted into each round bottom tube. Anti-human IgM F(ab)<sup>2</sup> was added to a final concentration of 0, 0.8, 1.7, 3.5, 7, or 14 µg/ml immediately prior to flow cytometry analysis and a temperature shift to 37°C. Cells were incubated at 37°C and analyzed every 10 min post-F(ab)<sup>2</sup> addition for up to 60 min. Gates were drawn to isolate singlet, live (eFluor450 negative) cells.

BCR internalization was measured by tracking the pH-induced decrease in FITC fluorescence that occurs as the BCR-bound FITC-conjugated F(ab) is internalized and trafficked into low pH endosomal compartments. To account for the change in fluorescence that may result from dissociation of fluorophore-conjugated F(ab) from the B cell surface over time, the change in FITC signal was corrected for the measured decrease in the fluorescence of the pH-insensitive fluorophore, Alexa Fluor 647. BCR internalization plots are presented as the negative change in FITC fluorescence relative to that of Alexa Fluor 647 and are calculated as follows:

$$-\frac{\Delta F_{corr}}{F} = -\frac{(I_{FITC} - I_{F0}) - \left[ I_{F0} \times \frac{(I_{AF647} - I_{AF0})}{I_{AF0}} \right]}{I_{F0}}$$

where  $I_{FITC}$  is the cell population mean fluorescence intensity (MFI) in the FITC channel at time of measurement,  $I_{F0}$  is the initial MFI of the cell population in the FITC channel,  $I_{AF647}$  is the cell population MFI in the Alexa Fluor 647 channel at time of measurement, and  $I_{AF0}$  is the initial MFI of the cell population in the Alexa Fluor 647 channel.

### Live cell confocal laser scanning microscopy

Imaging of BCR clustering and internalization in live cells in three dimensions was carried out using a Zeiss 880 confocal laser scanning microscope with a 63×, 1.4 NA oil-immersion Plan Apo DIC objective. DG-75 cells were prepared for imaging by spinning down 1 million cells at 200 × g for 5 min and resuspending the pellet in 100 µl of growth media with 1:1000 anti-human IgM-F(ab)-Alexa Fluor 488. Fluorescent labeling of the BCR was carried out at 4°C for 30 min. Cells were then diluted with 900 µl of imaging buffer, pelleted at 200 × g for 5 min, and resuspended in 150 µl IB. Approximately 300,000 labeled cells were allowed to settle for 5 min onto a cleaned, poly-lysine-treated, rinsed, coverslip assembled in an AttoFluor chamber (ThermoFisher: A7816) imaging chamber containing 600 µl of imaging buffer on a stage heated to 37°C inside an environmental control box. Regions containing multiple live, healthy cells were identified and the equatorial z-position was set as the origin. Two planes above and below this equatorial position were imaged, with a z-step size of 0.43 µm, encompassing a thickness of ~2.1 µm in the middle of the cell. After the addition of anti-human IgM F(ab)<sup>2</sup> to a final concentration of 12 µg/ml, this five slice stack was imaged once every 6 s for a total of 30 min using 488 nm excitation and detecting transmitted and emitted light using T-PMT and GaAsP detectors, respectively.

### Immunofluorescence imaging of BCR, actin, and clathrin

To observe endogenous clathrin relative to BCR on the plasma membrane, DG-75 cells were harvested at a concentration of 1–1.5 M cells/ml and spun down at 200 × g for 5 min. The cell pellet was resuspended at 10 million cells/ml in growth medium containing

1:5000 anti-human IgM F(ab)-Alexa Fluor 594. Cells were labeled for 30 min at 4°C followed by a 5-fold dilution in growth medium and centrifugation at 200 × g for 5 min. The labeled cell pellet was resuspended in growth medium to achieve a density of 2 million cells/ml, and anti-human IgM F(ab)<sup>2</sup> was added to achieve a F(ab)<sup>2</sup> concentration of 2 or 8 µg/ml (or omitted for unstimulated cells). F(ab)<sup>2</sup>-stimulated cells were incubated at 37°C for 5 or 15 min before diluting the cells twofold with cold IB. Approximately 125,000 cells were allowed to settle for 12 min onto cleaned, poly-lysine-treated, rinsed coverslips in a six-well plate containing 2 ml IB per well. Coverslips were treated with 0.5% paraformaldehyde (PFA) (Electron Microscopy Sciences) in IB for 1 min before transferring them into 2% PFA in imaging buffer for 20 min. Fixed coverslips were washed with phosphate-buffered saline (PBS), permeabilized by the addition of a solution of 0.5% Triton X-100 and 3% bovine serum albumin (BSA) in PBS for 2 min, and blocked in a solution of 0.2% Triton X-100 and 3% BSA in PBS for 1 h. Coverslips were incubated in primary mouse anti-clathrin heavy chain antibody X-22 (6 µg/ml in blocking buffer) for 1 h, washed with blocking buffer, and incubated with secondary donkey anti-mouse-Alexa Fluor 647 antibody (2 µg/ml) and phalloidin-Alexa Fluor 488 (33 nM) in blocking buffer for 1 h. After washing in blocking buffer and PBS, coverslips were fixed for 10 min in 2% PFA in PBS, rinsed in PBS, and stored at 4°C protected from light until imaging. Fixed, immunostained cells were imaged on the same Zeiss 880 confocal laser scanning microscope setup used for live cell imaging, using a 3-track program with excitation at 488, 561, and 633 nm. Z-stacks were collected to encompass the full cell volume.

### dSTORM

The superresolution localization method, dSTORM, was used to measure nanoscale changes in the size of BCR clusters on the plasma membrane following stimulation with anti-human IgM F(ab)<sup>2</sup>. DG-75 cells were prepared for imaging exactly as described for immunofluorescence imaging, but labeled with anti-human IgM F(ab)-Alexa Fluor 647 (1:5000 in growth medium) and without permeabilization or additional staining for clathrin or actin. Fixed, PBS washed coverslips were assembled in sealed AttoFluor imaging chambers (ThermoFisher) containing a freshly prepared dSTORM buffer (10% wt/vol D-glucose, 100 mM beta-mercaptoethanol, 0.8 mg/ml glucose oxidase, and 0.04 mg/ml catalase in PBS). Imaging was carried out as previously described in detail using a Nikon Eclipse Ti inverted microscope with a 100×, 1.49 NA objective and an Andor iXon Ultra 897 EM-CCD camera under the control of Nikon Elements NSTORM software (Sochacki and Taraska, 2017). STORM imaging was performed in TIRF, with 647-nm excitation at 75% laser power, collecting 10–20,000 frames with 10-ms exposure times. STORM images were processed as described previously, with the following modifications: a minimum height of 200 was used in the identification parameters for all images, and a value of 200 was used as the minimum number of photons during filtering. Drift correction was performed in Nikon Elements software, and Tiff images were rendered using a cross-representation with 8-nm pixel size. Localization precision was measured using Fourier shell correlation and measurement of individual localizations in the rendered Tiff image files, both of which yielded an apparent precision of ~27 nm.

To measure BCR cluster sizes from the STORM data, images were maximum filtered using a radius of 1 pixel (8 nm), and thresholded using the Li filter in Fiji/ImageJ (Schindelin et al., 2012) to produce a down-sampled, binary image, with a resolution of 40 nm. The result of this processing is to cluster localizations that are separated in space by a distance of less than the precision of the original image, 24 nm,

edge-to-edge—a conservative distance cutoff, which was empirically determined to identify reasonable clusters across the conditions tested, that is, monodisperse, small punctae in unstimulated cells, and heterogeneous, larger cluster sizes in stimulated cells. Six to 12 cells were analyzed for each condition, and the areas of all particles in the thresholded images were measured in Fiji/ImageJ. The total fluorescent area was measured for each cell, and the percentage of this area composed of small (<9600 nm<sup>2</sup>), intermediate (9600–48,000 nm<sup>2</sup>), and large (>48,000 nm<sup>2</sup>) fluorescent punctae was plotted in Origin (OriginLab). As described in *Results*, these area cutoffs were selected based on the typical size of clathrin-coated pits.

### Correlative superresolution fluorescence and electron microscopy

To directly visualize endocytic structures associated with BCR fluorescence, DG-75 cells were prepared for imaging exactly as described for STORM imaging above, with a few modifications. After 12 min of attachment to poly-L-lysine-coated gold fiducial coverslips (Hestzig, LLC) cells were fixed and "unroofed" to expose the cytoplasmic surface of the membrane adhered to the coverslip by squirting 4 ml of 0.75% PFA in stabilization buffer (70 mM KCl, 5 mM MgCl<sub>2</sub>, 30 mM HEPES, pH 7.4) steadily onto each coverslip using a 10-ml syringe with a 21G×1.5 needle, moving the stream over the coverslip at a right angle. After unroofing, coverslips were fixed in 2% PFA in stabilization buffer for 20 min, rinsed with PBS, treated with phalloidin-Alexa Fluor 488 (33 nM in PBS) for 10 min, and rinsed again in PBS prior to imaging.

Labeled, unroofed coverslips were assembled in sealed AttoFluor chambers containing freshly prepared dSTORM buffer. Imaging was performed as described above, with some additional steps to map cells on the coverslip for later correlation with TEM images. As described elsewhere (Sochacki *et al.*, 2017), a ~1 mm<sup>2</sup> region of the coverslip was initially mapped by montaging a 15 × 15 area in epifluorescence with excitation at 488 and 647 nm. These large montages of the phalloidin-Alexa Fluor 488 label were useful for reidentification of the cells imaged by STORM prior to imaging platinum replicas by TEM. After imaging five to eight cells, a 4-mm diameter circle was etched on the bottom of the coverslip with a diamond objective (Leica) to indicate the area of interest during sample processing for EM. Etched coverslips were cleaned of oil and fixed in a 2% solution of glutaraldehyde in PBS (Electron Microscopy Sciences).

As described previously (Sochacki *et al.*, 2017), coverslips were prepared for EM by treatment with 0.1% tannic acid solution for 20 min, rinsing with water, and staining with 0.1% uranyl acetate for 20 min. Coverslips were dehydrated using a Tousimis critical point dryer and coated with platinum and carbon in a JEOL freeze fracture device (Sochacki *et al.*, 2012). After locating cells of interest under a 10× phase-contrast objective, carbon-platinum replicas were separated from the underlying glass coverslip using 5% hydrofluoric acid and lifted onto glow-discharged formvar-coated 75 mesh copper grids for imaging on a JEOL 1400 TEM using SerialEM software for montaging (Mastronarde, 2005) at a magnification of 15,000×.

STORM images were processed as described above, but Tiff images were rendered using a Gaussian representation with 8-nm pixel size. STORM image files were transformed using custom MATLAB software to align images based on the measured coordinates of gold nanorods visible in both the rendered dSTORM Tiff files and TEM montages.

### DG-75 plasma membrane ferritin labeling

Cationized ferritin (49 mg) from horse spleen (Sigma-Aldrich F1897) was sonicated for 10–15 s and then added to 3 million DG-75 cells

for each condition. Samples were then gently swirled by hand to disperse ferritin. Next, the samples were incubated on ice for 10 min to allow the ferritin to adhere to cell membranes and then warmed at 37°C for 30 s. The samples were spun in a minicentrifuge in 10-s interval bursts to produce a pellet of approximately 2 mm × 3 mm. The unstimulated sample was then immediately fixed with 2.5% glutaraldehyde and 1% paraformaldehyde in 0.12 M sodium cacodylate buffer at pH 7.2 for 1 h at room temperature. The stimulated sample was resuspended in PBS and administered F(ab')<sub>2</sub> at a final concentration of 8 µg/ml and incubated for 15 min at 37°C. After incubation, stimulated cells were fixed in the same manner described for the unstimulated sample.

### Thin-section transmission electron microscopy

Fixed samples were washed 3× (20 min each) with 0.12 M sodium cacodylate buffer and stained with 1% osmium tetroxide (on ice and in the dark) for 1 h, washed twice (10 min each) in water, and stained with 1% uranyl acetate (overnight at 4°C). The following day samples were processed through a dehydration protocol of increasing concentrations of ethanol, infiltrated with Epon resin, and polymerized at 60°C for at least 48 h (VWR Symphony oven). Poststaining was determined to be not necessary due to sufficient contrast observed for ferritin; 65–70-nm ultrathin sections were obtained on a Leica-Reichert Ultracut microtome with a diamond knife (Delaware Diamond Knives) after each sample block resin was trimmed by a glass knife and confirmed to be in the cell layer through thick sectioning and Toluidine blue dye. Ultrathin sections were imaged on 200 mesh grids in a JEOL 1400 TEM.

### Analysis of EM and CLEM images

Platinum replica EM images of the entire visible plasma membrane of each cell were segmented by hand using ImageJ/FIJI with ROIs corresponding to the 1) total plasma membrane area, 2) CCS, 3) smooth raised membranes, and 4) gold fiducial particles. These ROIs were used to calculate density of structures, area of individual structures, Feret diameter of single structures, and nearest-neighbor distances between structures. Analysis, statistics, and plotting were done in Origin (OriginLab). The overlap pixel area between clathrin structures and SRMs was calculated from image masks made from ROIs in MATLAB (MathWorks).

The distribution and density of superresolution dSTORM fluorescence signal excluding regions 0.5 µm radius from gold fiducials were analyzed using the above EM-identified clathrin/SRM segmentation masks. Fluorescence signal within and surrounding a 200-nm radius of each segmented membrane structure was measured against the total fluorescence in the surrounding 1.8 µm radius area using Matlab. The resulting fluorescence ratio measurements for each structure in all experimental conditions were plotted in Origin (Originlab).

### SIM

Three-dimensional structured illumination images were collected on a DeltaVision OMX SR microscope with a 60× 1.42 NA oil emersion PSF objective. DG75 cells were transfected and stimulated as previously described and then fixed in 4% paraformaldehyde for 15 min. For staining with Alexa Fluor 594 phalloidin, the cells were additionally permeabilized with 0.1% Triton X-100 for 5 min, washed with PBS, and then incubated with Alexa Fluor 594 phalloidin diluted 1:50 in 1% BSA for 30 min. For 3D SIM image collection, z-stacks were taken at a focal plane near the cell membrane with a 0.125 µm z-step for a total of about 1.125 µm. Processed z-stacks collected in this way were then reconstructed in Image J using the 3D-Script plugin.

## Transfection and TIRF microscopy

Cells were transfected using a Lonza Nucleofector 2b device using the Amaxa Cell line Nucleofector Kit V (Cat. No. VCA-1003). Briefly,  $5 \times 10^6$  cells were harvested by spinning down at  $90 \times g$  for 10 min; 5  $\mu$ g of plasmid was mixed with Nucleofector solution and supplement following the manufacturer's protocol and then added to the pelleted cells. Cells were then transfected using the Nucleofector program M-013 and placed into warm media for overnight incubation. After 24 h, cells were stimulated and imaged on an inverted fluorescence microscope (IX-81; Olympus, Center Valley, PA) set up for TIRF imaging as described in Larson *et al.* (2014). Only healthy cells expressing levels moderate of transgene were selected for imaging. Previous studies in our lab have found no substantial effects of expression levels on co-localization values across the range of expression levels we commonly use in the lab (Larson *et al.*, 2014; Trexler *et al.*, 2016).

## ACKNOWLEDGMENTS

We thank the National Heart, Lung, and Blood Institute (NHLBI) Electron Microscopy core for support with EM imaging and instrumentation; Xufeng Wu and the NHLBI light Microscopy core for support with fluorescence imaging and instrumentation; the NHLBI FACS core for support with flow cytometry; and all members of the Taraska lab for comments and scientific dialogue. We thank Agila Somasundaram for critically reading the manuscript. We acknowledge Avital Rodal and Shiyu Wang for generously sending us plasmids with the FCHSD2-GFP gene. J.W.T. is supported by the Intramural Research Program, NHLBI, National Institutes of Health, Bethesda, Maryland.

## REFERENCES

- Aggeler J, Werb Z (1982). Initial events during phagocytosis by macrophages viewed from outside and inside the cell: membrane-particle interactions and clathrin. *J Cell Biol* 94, 613–623.
- Almeida-Souza L, Frank RAW, Garcia-Nafria J, Colussi A, Gunawardana N, Johnson CM, Yu M, Howard G, Andrews B, Vallis Y, *et al.* (2018). A flat BAR protein promotes actin polymerization at the base of clathrin-coated pits. *Cell* 174, 325–337.e314.
- Avalos AM, Meyer-Wentrup F, Ploegh HL (2014). B-cell receptor signaling in lymphoid malignancies and autoimmunity. *Adv Immunol* 123, 1–49.
- Batista FD, Iber D, Neuberger MS (2001). B cells acquire antigen from target cells after synapse formation. *Nature* 411, 489–494.
- Betzig E, Patterson GH, Sougrat R, Lindwasser OW, Olenych S, Bonifacino JS, Davidson MW, Lippincott-Schwartz J, Hess HF (2006). Imaging intracellular fluorescent proteins at nanometer resolution. *Science* 313, 1642–1645.
- Brown BK, Song W (2001). The actin cytoskeleton is required for the trafficking of the B cell antigen receptor to the late endosomes. *Traffic* 2, 414–427.
- Chapman CJ, Zhou JX, Gregory C, Rickinson AB, Stevenson FK (1996). VH and VL gene analysis in sporadic Burkitt's lymphoma shows somatic hypermutation, intraclonal heterogeneity, and a role for antigen selection. *Blood* 88, 3562–3568.
- Cheng PC, Dykstra ML, Mitchell RN, Pierce SK (1999). A role for lipid rafts in B cell antigen receptor signaling and antigen targeting. *J Exp Med* 190, 1549–1560.
- Clark MR, Massenbun D, Siemasko K, Hou P, Zhang M (2004). B-cell antigen receptor signaling requirements for targeting antigen to the MHC class II presentation pathway. *Curr Opin Immunol* 16, 382–387.
- Cleyrat C, Darehshoury A, Anderson KL, Page C, Lidke DS, Volkman N, Hanein D, Wilson BS (2013). The architectural relationship of components controlling mast cell endocytosis. *J Cell Sci* 126, 4913–4925.
- Conner SD, Schmid SL (2003). Regulated portals of entry into the cell. *Nature* 422, 37–44.
- Dambournet D, Sochacki KA, Cheng AT, Akamatsu M, Taraska JW, Hockemeyer D, Drubin DG (2018). Genome-edited human stem cells expressing fluorescently labeled endocytic markers allow quantitative analysis of clathrin-mediated endocytosis during differentiation. *J Cell Biol* 217, 3301–3311.
- Davis RE, Ngo VN, Lenz G, Tolar P, Young RM, Romesser PB, Kohlhammer H, Lamy L, Zhao H, Yang Y, *et al.* (2010). Chronic active B-cell-receptor signalling in diffuse large B-cell lymphoma. *Nature* 463, 88–92.
- Ferreira APA, Boucrot E (2018). Mechanisms of carrier formation during clathrin-independent endocytosis. *Trends Cell Biol* 28, 188–200.
- Freeman SA, Lei V, Dang-Lawson M, Mizuno K, Roskelley CD, Gold MR (2011). Cofilin-mediated F-actin severing is regulated by the Rap GTPase and controls the cytoskeletal dynamics that drive lymphocyte spreading and BCR microcluster formation. *J Immunol* 187, 5887–5900.
- Hao S, August A (2005). Actin depolymerization transduces the strength of B-cell receptor stimulation. *Mol Biol Cell* 16, 2275–2284.
- Harwood NE, Batista FD (2010). Early events in B cell activation. *Annu Rev Immunol* 28, 185–210.
- Heilemann M, van de Linde S, Schüttelpelz M, Kasper R, Seefeldt B, Mukherjee A, Tinnefeld P, Sauer M (2008). Subdiffraction-resolution fluorescence imaging with conventional fluorescent probes. *Angew Chem Int Ed Engl* 47, 6172–6176.
- Hoogeboom R, Tolar P (2016). Molecular Mechanisms of B Cell Antigen Gathering and Endocytosis. *Curr Top Microbiol Immunol* 393, 45–63.
- Ketchum C, Miller H, Song W, Upadhyaya A (2014). Ligand mobility regulates B cell receptor clustering and signaling activation. *Biophys J* 106, 26–36.
- Kopeck BG, Paez-Segala MG, Shtengel G, Sochacki KA, Sun MG, Wang Y, Xu CS, van Engelenburg SB, Taraska JW, Looger LL, *et al.* (2017). Diverse protocols for correlative super-resolution fluorescence imaging and electron microscopy of chemically fixed samples. *Nat Protoc* 12, 916–946.
- Larson BT, Sochacki KA, Kindem JM, Taraska JW (2014). Systematic spatial mapping of proteins at exocytic and endocytic structures. *Mol Biol Cell* 25, 2084–2093.
- Lee J, Sengupta P, Brzostowski J, Lippincott-Schwartz J, Pierce SK (2017). The nanoscale spatial organization of B-cell receptors on immunoglobulin M- and G-expressing human B-cells. *Mol Biol Cell* 28, 511–523.
- Lessard CJ, Sajuthi S, Zhao J, Kim K, Ice JA, Li H, Ainsworth H, Rasmussen A, Kelly JA, Marion M, *et al.* (2016). Identification of a Systemic Lupus Erythematosus Risk Locus Spanning ATG16L2, FCHSD2, and P2RY2 in Koreans. *Arthritis Rheumatol* 68, 1197–1209.
- Liu C, Miller H, Orlowski G, Hang H, Upadhyaya A, Song W (2012). Actin reorganization is required for the formation of polarized B cell receptor signalosomes in response to both soluble and membrane-associated antigens. *J Immunol* 188, 3237–3246.
- Mastrorade DN (2005). Automated electron microscope tomography using robust prediction of specimen movements. *J Struct Biol* 152, 36–51.
- Matsuda F, Shin EK, Nagaoka H, Matsumura R, Haino M, Fukita Y, Taka-ishi S, Imai T, Riley JH, Anand R, *et al.* (1993). Structure and physical map of 64 variable segments in the 3'0.8-megabase region of the human immunoglobulin heavy-chain locus. *Nat Genet* 3, 88–94.
- Mayor S, Parton RG, Donaldson JG (2014). Clathrin-independent pathways of endocytosis. *Cold Spring Harb Perspect Biol* 6, <https://doi.org/10.1101/cshperspect.a016758>.
- McMahon HT, Boucrot E (2011). Molecular mechanism and physiological functions of clathrin-mediated endocytosis. *Nat Rev Mol Cell Biol* 12, 517–533.
- Mettlen M, Chen PH, Srinivasan S, Danuser G, Schmid SL (2018). Regulation of clathrin-mediated endocytosis. *Annu Rev Biochem* 87, 871–896.
- Natkanski E, Lee WY, Mistry B, Casal A, Molloy JE, Tolar P (2013). B cells use mechanical energy to discriminate antigen affinities. *Science* 340, 1587–1590.
- Pierce SK, Liu W (2010). The tipping points in the initiation of B cell signaling: how small changes make big differences. *Nat Rev Immunol* 10, 767–777.
- Ringstad N, Nemoto Y, De Camilli P (1997). The SH3p4/SH3p8/SH3p13 protein family: Binding partners for synaptojanin and dynamin via a Grb2-like Src homology 3 domain. *Proc Natl Acad Sci* 94, 8569–8574.
- Rodal AA, Motola-Barnes RN, Littleton JT (2008). Nervous wreck and Cdc42 cooperate to regulate endocytic actin assembly during synaptic growth. *J Neurosci* 28, 8316–8325.
- Salisbury JL, Condeelis JS, Satir P (1980). Role of coated vesicles, microfilaments, and calmodulin in receptor-mediated endocytosis by cultured B lymphoblastoid cells. *J Cell Biol* 87, 132–141.
- Schindelin J, Arganda-Carreras I, Frise E, Kaynig V, Longair M, Pietzsch T, Preibisch S, Rueden C, Saalfeld S, Schmid B, *et al.* (2012). Fiji: an open-source platform for biological-image analysis. *Nat Methods* 9, 676–682.
- Scott BL, Sochacki KA, Low-Nam ST, Bailey EM, Luu Q, Hor A, Dickey AM, Smith S, Kerkvliet JG, Taraska JW, *et al.* (2018). Membrane bending occurs at all stages of clathrin-coat assembly and defines endocytic dynamics. *Nat Commun* 9, 419.

- Sezgin E, Levental I, Mayor S, Eggeling C (2017). The mystery of membrane organization: composition, regulation and roles of lipid rafts. *Nat Rev Mol Cell Biol* 18, 361–374.
- Sigismund S, Argenzio E, Tosoni D, Cavallaro E, Polo S, Di Fiore PP (2008). Clathrin-mediated internalization is essential for sustained EGFR signaling but dispensable for degradation. *Dev Cell* 15, 209–219.
- Siraganian RP, de Castro RO, Barbu EA, Zhang J (2010). Mast cell signaling: the role of protein tyrosine kinase Syk, its activation and screening methods for new pathway participants. *FEBS Lett* 584, 4933–4940.
- Sochacki KA, Dickey AM, Strub MP, Taraska JW (2017). Endocytic proteins are partitioned at the edge of the clathrin lattice in mammalian cells. *Nat Cell Biol* 19, 352–361.
- Sochacki KA, Larson BT, Sengupta DC, Daniels MP, Shtengel G, Hess HF, Taraska JW (2012). Imaging the post-fusion release and capture of a vesicle membrane protein. *Nat Commun* 3, 1154.
- Sochacki KA, Shtengel G, van Engelenburg SB, Hess HF, Taraska JW (2014). Correlative super-resolution fluorescence and metal-replica transmission electron microscopy. *Nat Methods* 11, 305–308.
- Sochacki KA, Taraska JW (2017). Correlative fluorescence super-resolution localization microscopy and platinum replica EM on unroofed cells. *Methods Mol Biol* 1663, 219–230.
- Souwer Y, Griekspoor A, Jorritsma T, de Wit J, Janssen H, Neefjes J, van Ham SM (2009). B cell receptor-mediated internalization of salmonella: a novel pathway for autonomous B cell activation and antibody production. *J Immunol* 182, 7473–7481.
- Srinivas Reddy A, Tsourkas PK, Raychaudhuri S (2011). Monte Carlo study of B-cell receptor clustering mediated by antigen crosslinking and directed transport. *Cell Mol Immunol* 8, 255–264.
- Srinivasan S, Burckhardt CJ, Bhave M, Chen Z, Chen PH, Wang X, Danuser G, Schmid SL (2018). A noncanonical role for dynamin-1 in regulating early stages of clathrin-mediated endocytosis in non-neuronal cells. *PLoS Biol* 16, e2005377.
- Stoddart A, Jackson AP, Brodsky FM (2005). Plasticity of B cell receptor internalization upon conditional depletion of clathrin. *Mol Biol Cell* 16, 2339–2348.
- Stone MB, Shelby SA, Nunez MF, Wissner K, Veatch SL (2017). Protein sorting by lipid phase-like domains supports emergent signaling function in B lymphocyte plasma membranes. *Elife* 6.
- Taylor MJ, Perrais D, Merrifield CJ (2011). A high precision survey of the molecular dynamics of mammalian clathrin-mediated endocytosis. *PLoS Biol* 9, e1000604.
- Thyagarajan R, Arunkumar N, Song W (2003). Polyvalent antigens stabilize B cell antigen receptor surface signaling microdomains. *J Immunol* 170, 6099–6106.
- Tolar P (2017). Cytoskeletal control of B cell responses to antigens. *Nat Rev Immunol* 17, 621–634.
- Tomas A, Futter CE, Eden ER (2014). EGF receptor trafficking: consequences for signaling and cancer. *Trends Cell Biol* 24, 26–34.
- Treanor B, Depoil D, Bruckbauer A, Batista FD (2011). Dynamic cortical actin remodeling by ERM proteins controls BCR microcluster organization and integrity. *J Exp Med* 208, 1055–1068.
- Treanor B, Depoil D, Gonzalez-Granja A, Barral P, Weber M, Dushek O, Bruckbauer A, Batista FD (2010). The membrane skeleton controls diffusion dynamics and signaling through the B cell receptor. *Immunity* 32, 187–199.
- Trexler AJ, Sochacki KA, Taraska JW (2016). Imaging the recruitment and loss of proteins and lipids at single sites of calcium-triggered exocytosis. *Mol Biol Cell* 27, 2423–2434.
- Trexler AJ, Taraska JW (2017). Two-Color total internal reflection fluorescence microscopy of exocytosis in endocrine cells. *Methods Mol Biol* 1563, 151–165.
- Trombetta ES, Mellman I (2005). Cell biology of antigen processing in vitro and in vivo. *Annu Rev Immunol* 23, 975–1028.
- Watanabe S, Boucrot E (2017). Fast and ultrafast endocytosis. *Curr Opin Cell Biol* 47, 64–71.
- Wilson BS, Pfeiffer JR, Oliver JM (2002). FcεRI signaling observed from the inside of the mast cell membrane. *Mol Immunol* 38, 1259–1268.
- Zhu Q, Zhang M, Shi M, Liu Y, Zhao Q, Wang W, Zhang G, Yang L, Zhi J, Zhang L, et al. (2016). Human B cells have an active phagocytic capability and undergo immune activation upon phagocytosis of *Mycobacterium tuberculosis*. *Immunobiology* 221, 558–567.